Note: Snapshot PDF is the proof copy of corrections marked in EditGenie, the layout would be different from typeset PDF and EditGenie editing view.

Author Queries & Comments:

Q1 : Please note that the Funding section has been created by summarising information given in acknowledgements/CATS.

Please correct if this is inaccurate.

Response: Resolved

Q2: The disclosure statement has been inserted. Please correct if this is inaccurate.

Response: Resolved

Q3: Please provide missing city for the reference "[33]" references list entry.

Response: Resolved

Q4: Please provide missing city for the reference "[35]" references list entry.

Response: Resolved

Q5: Please provide missing city for the reference "[36]" references list entry.

Response: Resolved

Effect of oxidation on the thermal expansion of a refractory multicomponent alloy

PHILOSOPHICAL MAGAZINE LETTERS

E. OSEI-AGYEMANG AND G. BALASUBRAMANIAN

Eric Osei-Agyemang, D Ganesh Balasubramanian

Department of Mechanical Engineering and Mechanics, Lehigh University, Bethlehem, PA, USA

CONTACT Ganesh Balasubramanian bganesh@lehigh.edu, gab317@lehigh.edu Packard Laboratory 561, 19 Memorial Drive West, Bethlehem, PA 18015, USA

History: received: 2020-9-11 accepted: 2021-1-20

Copyright Line: © 2021 Informa UK Limited, trading as Taylor & Francis Group

ABSTRACT

We employ first-principles calculations to examine the role of oxidation on the thermal expansion behaviour of a refractory multicomponent alloy. Our results reveal that the linear expansion and the coefficient of volumetric expansion over a range of temperatures have higher values for the oxidised alloy than the pure material. The enhanced expansion for the oxidised alloy is attributed to significant changes in the lattice parameter of the alloy upon surface oxidation. During oxidation, the diffusion of oxygen atoms to the subsurface layer of the alloy after complete surface coverage produces a displacement of the constituent elements that form metal oxides. This depletion creates vacancy sites in the lattice for enabling enhanced expansivity in the oxidised structure relative to the pure refractory alloy.

KEYWORDS

- Thermal expansion
- refractory alloys
- first principles calculations
- oxidation

FUNDING

This **[Q1]** material is based on the work supported, in part, by the National Science Foundation (NSF) under Award No. CMMI-1944040; Division of Civil, Mechanical and Manufacturing Innovation.

Refractory multi-principal element alloys (RMPEAs) are being considered as potential candidates to address the need for high-

performance alloys with notable mechanical properties for applications in extreme temperatures and harsh operating conditions [1–5]. These alloys typically consist of four or more principal elements, each with a concentration between 5 and 35 atom per cent [6]. Though ordered phases and intermetallics do form for certain compositions, the predominant phases of MPEAs are characteristically disordered solid solutions, generally in the face-centered cubic (FCC) or body-centered cubic (BCC) crystallographic forms. The high configurational entropy of mixing, $\Delta S_{conf} = -R\sum X_i \ln(X_i) \ge 1.5R$, where X_i represents the atom fraction of element i and R is the molar gas constant [7,8], favours the formation of the disordered over the ordered phases [8–11]. Nonetheless, the high entropy of mixing in equiatomic MPEAs retards the formation of intermetallics [12]. Moreover, the formation of intermetallic phases is favoured by large atomic size mismatch and large negative enthalpies of mixing of the alloying elements [13,14].

The high level of interest in MPEAs from the research community in recent years is attributed to the various notable properties of these materials relative to conventional alloys. MPEAs have been reported to possess superior mechanical properties such as high strength, hardness, and creep resistance [6,15,16]. In a recent study [15], an equiatomic CoCrNiFeNb MPEA was prepared by a combination of short-term mechanical alloying (MA) followed by compaction through spark plasma sintering (SPS). The authors observed that the alloys prepared by a combination of MA and SPS yielded ultrafine-grained microstructures relative to those prepared by induction melting. Subsequently, such combined processing resulted in a higher ultimate compressive strength and hardness, outperforming other similar alloys. In another study, a combinatorial approach was used to develop a database to examine the oxidation resistance of Al_xCr_yMo_zNbTiZr refractory MPEAs [17]. The results revealed that, in order to improve the oxidation resistance, the Zr content had to be reduced to 10 at.%, while the Al, Ta, and V fractions were varied to obtain an optimal combination of oxidation resistance and mechanical properties [18,19]. The review by Zhang et al. [20] provides a thorough discussion on the formation criteria of MPEAs as compared to traditional alloys. The thermodynamics guiding the formation and stability of these MPEAs over dilute solid-solution alloys is presented as well as a discussion of the role of processing methods such as arc melting, inductive melting, sputter, laser cladding, and electrochemical methods. Recently, Brechtl et al. [21] examined the serrated flow occurring in MPEAs during mechanical deformation and asserted that the phenomenon, dependent on the strain rate and temperature, contributed significantly to microstructural changes in the alloy.

In the realm of high-temperature applications, RMPEAs are being considered as potential alternatives for Ni-based superalloys, with several possible compositions being suggested [6,10,16,22–27]. While the predominant phase in most of these RMPEAs is BCC, in essence these alloys are comprised of three or less crystallographic phases [12]. Recently, a refractory alloy (Mo_{0.5}W_{0.5})_{0.85}Ta_{0.10}(TiZr)_{0.05}, subsequently referred to here simply as pRMPEA (*p* denotes 'pure'), was shown to exhibit an enhanced elastic modulus (3× at 300 K) over equiatomic alloys composed of the same elements, and an over 20% greater modulus at 2000 K compared to commercial alloys [28]. The feasibility of this and similar MPEAs for operations at high temperatures is dependent on their oxidation resistance and volumetric coefficient of thermal expansion (CTE). However, the literature on the surface and internal degradation mechanisms of MPEAs is sparse [1,29–32]. Here, we employ first-principles calculations to understand the effect of initial chemisorption of oxygen on the CTE of pRMPEA. We investigate a composite structure with an oxide layer on top of the MPEA that subsequently leads to a metal-depleted alloy, as described in our earlier report [1]. We also consider oxygen atoms at the subsurface level of the exposed alloy structure. The alloy with a completely oxidised surface is denoted as oRMPEA. As elaborated below, we find that oRMPEA assumes higher CTE values than the pRMPEA, posing increased challenges for their applications at elevated temperatures.

Quasi-harmonic approximation: Since the crystal potential is an anharmonic function of volume, the phonon properties change when the volume is varied, and this volume dependence of phonon properties is encompassed within the quasi-harmonic approximation (QHA). In the harmonic approximation, the dynamical properties of atoms are obtained through the solution of an eigenvalue problem of the dynamical matrix [33–36] D(i) as

where

Here m_l is the mass of atom l, q is the wave vector, and i is the band index. The phonon frequency and the polarisation vector of the phonon mode are denoted by ω_{qi} and e_{qi} , respectively. The eigenvalues ω_{qi} of D(q) are real since the latter is a Hermitian matrix. The energy E of a system of phonons can be calculated from the canonical distribution under the harmonic approximation when the phonon frequencies over the Brillouin zone are known. Thus,

Here T, k_B and \hbar are the temperature, the Boltzmann constant and the reduced Planck constant, respectively. Several thermodynamic properties such as the entropy S, the Helmholtz free energy of phonons F, and the heat capacity at constant volume C_v can be obtained from the energy distribution in Equation (3) [36].

In the QHA, the variation of the phonon frequency modes with respect to volume is the mode-Grüneisen parameter \gamma _{qi}\lpar V \rpar with the slope of this variation normalised. \gamma _{qi}\lpar V \rpar is calculated from the volume derivative of the dynamical matrix as [34]

The mode contributions to the heat capacity C_{qi} can be employed to relate $\gamma_{qi} = \sqrt{qi} \operatorname{sgmma} (qi) \operatorname{gmma} (qi)$

 $\label{linear large displays tyle { \Sigma _ {qi} C_{qi}} \operatorname{C_v} \eqno \label{linear large displays tyle } \\ 8 \operatorname{C_v} \eqno \label{linear large displays tyle } \\$

\gamma _{qi}\|par V \rpar is a measure of the anharmonicity of the phonon modes and is directly related to the third-order force constants. Hence, crystals with large anharmonic terms can result in a non-linear relation between phonon frequencies and the volume [34]. Large \gamma _{qi}\|par V \rpar values are observed for alloys that exhibit structural phase transitions [37].

For solids, the Gibbs free energy

G\lpar {T\comma \; p} \rpar = {\rm \; }\mathop {\min }\limits v \lsqb {U\lpar V \rpar

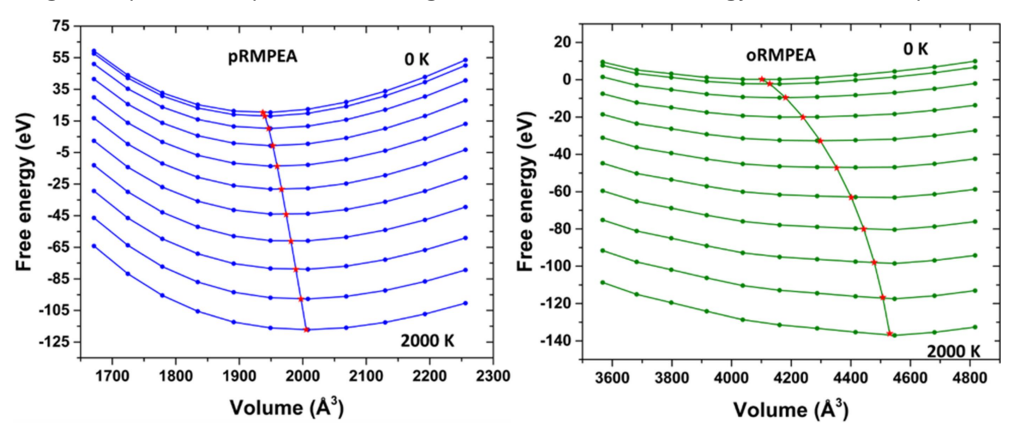
Here, p and V are the corresponding pressure and volume, U(V) is the internal energy calculated as the total electronic energy at constant volume, and $F_{phonon}(T;V)$ denotes the Helmholtz free energy of phonons at temperature T and volume V. Hence, using V(T, p) as the equilibrium volume at T and P, the heat capacity at constant pressure C_p can be calculated from the Gibbs free energy as

 $C_P \left \{ \text{T} \right ^2G \right ^2G \left \{ \text{T} \right ^2G \left \{ \text{T} \right ^2G \right ^2G \right ^2G \left \{ \text{T} \right ^2G \left \{ \text{T} \right ^2G \left \{ \text{T} \right ^2G \right ^2G \right ^2G \left \{ \text{T} \right ^2G \left \{ \text{T} \right ^2G \left \{ \text{T} \right ^2G \right ^2G \left \{ \text{T} \right ^2G \left \{ \text{T}$

We use the Vienna ab initio Simulation Package (VASP) [38] based on Mermin's finite-temperature DFT [39] to perform all the calculations. The electronic configurations used to represent the Mo, W, Ta, Ti, Zr and O atoms are [Kr] $4d^55s^1$, [Xe] $4f^145d^46s^2$, [Xe] $4f^145d^36s^2$, [Ar] $3d^24s^2$, [Kr] $4d^25s^2$, and [He] $2s^22p^4$, respectively. The Projector Augmented Wavefunction (PAW) pseudopotentials [40] are used to represent the core electrons as well as the core part of the valence electron wavefunctions that are kept frozen. The PAW representation reduces the number of planewaves required to effectively describe the electrons close to the nuclei. The generalised gradient approximation (GGA) exchange correlation functional, as parametrised by Perdew, Burke and Ernzerhof (PBE) [41], is used while employing the Methfessel-Paxton [42] smearing scheme by setting the gamma parameter to 0.1 eV. An energy cut-off of 600 eV is used for the planewaves expansion. A Monkhorst–Pack [43] special grid sampling of the k-points for integration of the Brillouin zone yields $4 \times 4 \times 4$ k-points representing 36 irreducible number of sampling points for all bulk calculations. The self-consistent field procedure is used for resolution of the Kohn–Sham equations by setting energy changes for each cycle at 10^{-4} eV as the convergence criterion between two successive iterations. The random solid-solution lattice structures used for the pure and oxidised alloys are generated with the special quasi-random structures (SQS) [44] method. The details for such generations are available elsewhere [1]. All phonon calculations are performed using the supercell approach, while the force constants in the supercells are used in obtaining phonon frequencies through the PHONOPY code [37]. We use a $1 \times 1 \times 1$ supercell in the QHA calculations with a finite displacement of 0.01 Å.

Figure 1 displays the curves for the thermodynamic Gibbs free energies for both the pure and oxidised RMPEAs across a temperature range from 0 to 2000 K. The calculated free-energy minima at all temperatures are achieved at considerably higher volumes for the oRMPEA relative to the pRMPEA. Note that both alloys could achieve higher volumes (V) in the process of minimising the Gibbs free energy of the system. We anticipate differences in volumetric expansions and other thermodynamic properties for pRMPEA and oRMPEA.

Figure 1. Gibbs free energy $[U(V) + F_{phonon}(T;V)]$ at p = 0 as a function of unit cell volume for pRMPEA (left) and oRMPEA (right). The filled circles denote the calculated free-energy points at every 200 K between 0 and 2000 K. The minimum values of the fitted Gibbs free energy in Equation (9) are represented as solid red stars at the respective temperatures and the line connecting these points is to provide a visual guide to the Gibbs free-energy minima as temperature is increased.



The linear expansion for the RMPEAs, presented in Figure 2a, is calculated as $\Delta L/L_0$ where L = Voot(3) of V. L_0 is the value of L at 300 K, while $\Delta L = L - L_0$. Below room temperature, the pRMPEA exhibits a relatively higher expansion but beyond 300 K the oRMPEA exhibits enhanced linear extension. For instance, at 1500 K, oRMPEA reveals an expansion L that of the pRMPEA. The

change in the expansion with temperature is steeper for the oRMPEA, with that for the pRMPEA increasing only marginally with temperature. The greater linear expansion for the oxidised alloy arises from significant changes in the lattice parameter of the alloy upon surface oxidation. The lattice parameter of an RMPEA is calculated as the weighted average of the lattice constants of the constituent elements in the alloy. In our previous study, we observed the initial point of oxygen attack on the alloy surface as being at Zr sites [1]. Note that we consider only the initial stage of oxygen adsorption on the surface of the MPEA rather than a complete structural transition. Further oxygen addition leads to penetration of O atoms into the subsurface layer, resulting in the subsequent formation of Zr oxides while Zr atoms are depleted from the lattice structure. This process produces pockets of spaces in the resulting lattice of the oxidised structure for further volumetric expansion. As such, we expect the coefficient of linear thermal expansion to strongly increase at higher temperatures and not to attain an almost linear behaviour above room temperature.

Figure 2. The calculated (a) linear expansion $\Delta L/L_0$ (L = voot 3 of V rpar as a function of temperature for the pure pRMPEA and the oRMPEA, (b) the variations of bulk moduli with temperature, (c) the changes in the heat capacity at constant pressure C_p , and (d) the evolution of the volumetric thermal expansion coefficient at different temperatures for the pRMPEA and oRMPEA.

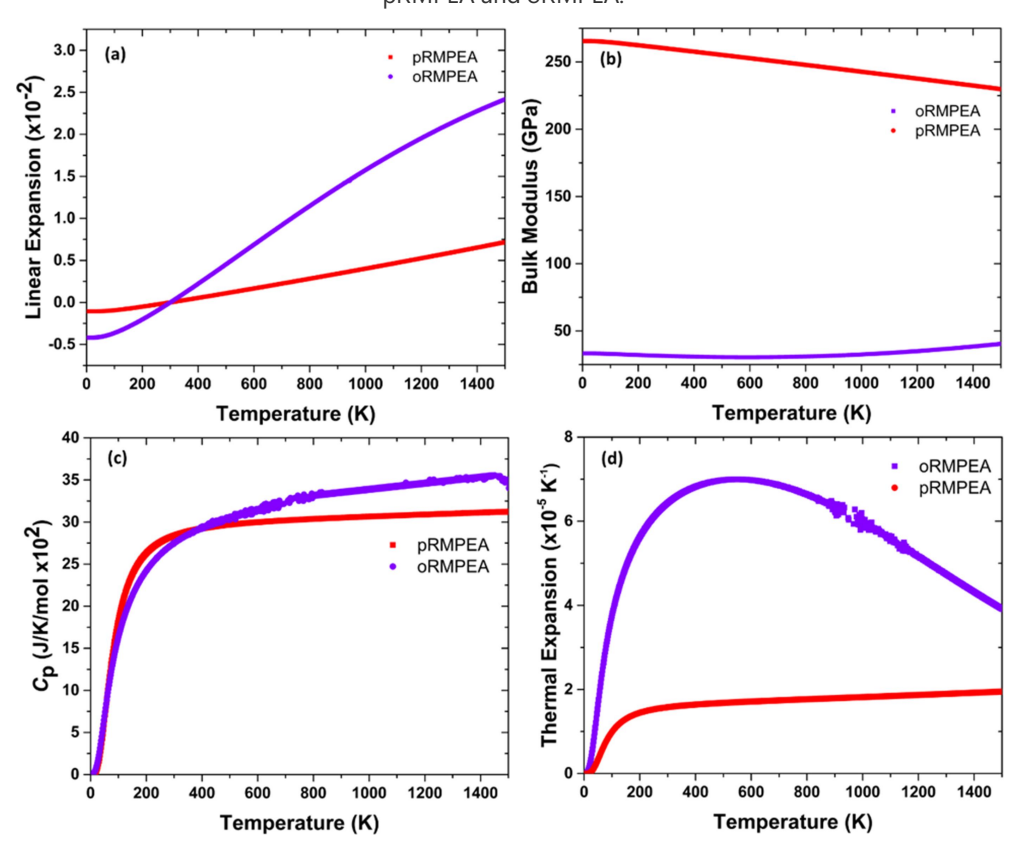


Figure 2b displays the isothermal bulk moduli as a function of temperature. At all temperatures, the bulk modulus for the pRMPEA is about 5× that of the oRMPEA. For the pRMPEA, the bulk modulus marginally softens from 0 to 1500 K, while it remains fairly constant from 0 to 800 K for the oRMPEA and increases only slightly above 800 K up to 1500 K. At 300 K, the pRMPEA exhibits a high bulk modulus of ~270 GPa while that of the oRMPEA is ~35 GPa. pRMPEA is thus highly resistant to compression compared to oRMPEA. As a comparison, the experimental bulk modulus for some high-temperature refractory MPEAs such as NbTaHfZrTi is 134.6 GPa [45], NbMoTaWTi is 139 GPa [46], and NbMoTaWTiV is 150 GPa [46]. These measurements are suggestive of the high compression resistance of pRMPEA relative to other refractory MPEAs. During the oxidation process, we observe movement of O atoms to the subsurface layer of the alloy upon full coverage with displacement of the constituent elements (beginning with Zr) to form metal oxides [1]. This depletion creates vacancy sites in the lattice for permissible compressibility in the oxidised structure compared to the pure refractory alloy.

The heat capacities at constant pressure C_p for the pure and oxidised RMPEAs are reproduced in Figure 2c. Below 100 K, the C_p values for both pRMPEA and oRMPEA are identical. However, variations are noted between 100 and 300 K where the pRMPEA exhibits higher C_p values than the oRMPEA. The trend however changes at temperatures greater than 300 K where the oRMPEA shows higher C_p values than the pRMPEA. Above room temperature, the significant amount of oxide layer formed retains much of the supplied heat in addition to the bulk material. Above 1500 K, the C_p value for oRMPEA begins to decrease owing to the removal of some surface oxide material as noted previously [1].

The calculated CTE for pRMPEA and oRMPEA, shown in Figure 2d, demonstrate that oRMPEA exhibits higher CTE values than

pRMPEA at all temperatures. For the pRMPEA, CTE increases rapidly up to ~150 K and remains constant at temperatures above 200 K. Additionally, the pRMPEA CTE increases from 0 K to ~15 × 10^{-6} K⁻¹ before saturating, while the CTE for the oRMPEA increases rapidly to ~70 × 10^{-6} K⁻¹ at 500 K but subsequently decreases gradually. This difference in the CTE predictions can be correlated to a reduction in the lattice parameter of the oxidised alloy caused by the removal of Zr, Ti, Mo, W and Ta atoms to form their respective oxides. This reduction in the lattice parameter manifests in the susceptibility of the alloy for lattice expansion. We estimate an initial reduction in the lattice parameter by ~2.4% caused by oxidisation of the alloy and the initial depletion of Zr atoms. As a comparison, the experimental CTE for ZrO_2 in the monoclinic phase is 17×10^{-6} K⁻¹ [47]. The difference in the CTE of ZrO_2 as compared to oRMPEA arises from the expansion of the unoxidised regions in the alloy. As O atoms move to subsurface layers of the bulk material, there is the possibility of formation of volatile Mo and W oxides which augments the potential for further elemental depletion from the bulk structure, akin to a similar phenomenon reported previously in an aged Inconel 718 alloy with subsequent formation of an oxide later [48]. It is important to note that a scrutiny of the crystallographic phases of the different oxides formed by the constituent elements of the alloy may reveal the structures to be non-cubic; therein anisotropy in the thermal expansion properties is quite possible.

In summary, we examine the thermal expansion of pure (pRMPEA) and oxidised (oRMPEA) forms of a multicomponent alloy as a function of temperature by combining first-principles calculations with phonon models. We calculate the linear expansion of the oRMPEA to be significantly higher than for pRMPEA at temperatures above 300 K. From the compressibility predictions for the two MPEA materials, we find that the oxidised sample is the most compressible at all temperatures compared to its pure-form counterpart. The isothermal bulk modulus for pRMPEA decreases gradually with temperature while it persists with a constant value for the oRMPEA. Though pRMPEA assumes higher C_p values at lower temperatures, oRMPEA maintains a higher C_p at elevated temperatures. From the predictions of the volumetric thermal expansion coefficient, we find that oRMPEA exhibits higher values across a wide temperature range relative to pRMPEA, with a subsequent reduction as the oxygen diffuses to the subsurface layers of the bulk alloy. Hence, since the oxidised alloys have higher expansion coefficients, their application to high-temperature operations could be challenging unless the material is tuned to limit the expansion and prevent mismatch with other components of the system.

This work provides an initial analysis and guidance for future theoretical and experimental studies on the effect of oxidation on the thermal properties of MPEAs. Additionally, it raises more questions for subsequent investigation of the different oxides that are formed by the constituent elements, the resulting vacancies due to metal atom depletion, and the effect on the physical and mechanical properties of these MPEAs under extreme conditions.

Acknowledgments

This material is based on the work supported, in part, by the National Science Foundation (NSF) under Award No. CMMI-1944040. Any opinions, findings, conclusions or recommendations expressed in this material are those of the authors and do not necessarily reflect the views of the NSF.

Disclosure statement

No potential conflict of interest was reported by the author(s [Q2]).

Data availability statement

The data reported in this paper is available from the corresponding author upon reasonable request.

ORCID

Ganesh Balasubramanian http://orcid.org/0000-0003-1834-5501

References

- 1 E. Osei-Agyemang and G. Balasubramanian, npj Mater. Degrad. 3 (2019) p.20.
- 2 E.P. George, D. Raabe and R.O. Ritchie, Nat. Rev. Mater. 4 (2019) pp.515–534.
- **3 D. Miracle and O. Senkov**, Acta Mater. 122 (2016) pp.448–511.
- 4 D.B. Miracle, JOM 69 (2017) pp.2130-2136.
- **5 D.B. Miracle**, Nat. Commun. 10 (2019) p.1805.
- **6** J.-W. Yeh, S.-K. Chen, S.-J. Lin, J.-Y. Gan, T.-S. Chin, T.-T. Shun, C.-H. Tsau and S.-Y. Chang, Adv. Eng. Mater. 6 (2004) pp.299–303.
- **7 J.-W. Yeh**, JOM 65 (2013) pp.1759–1771.

- 8 D. Miracle, J. Miller, O. Senkov, C. Woodward, M. Uchic and J. Tiley, Entropy 16 (2014) pp.494–525.
- 9 S. Singh, N. Wanderka, B.S. Murty, U. Glatzel and J. Banhart, Acta Mater. 59 (2011) pp.182–190.
- 10 O.N. Senkov, S.V. Senkova, D.B. Miracle and C. Woodward, Mater. Sci. Eng. A 565 (2013) pp.51–62.
- 11 Y.P. Wang, B.S. Li and H.Z. Fu, Adv. Eng. Mater. 11 (2009) pp.641–644.
- 12 O. Senkov, D. Isheim, D. Seidman, A. Pilchak, O.N. Senkov, D. Isheim, D.N. Seidman and A.L. Pilchak, Entropy 18 (2016) pp.102.
- 13 Y. Zhang, X. Yang and P.K. Liaw, JOM 64 (2012) pp.830–838.
- 14 Y. Zhang, Y.J. Zhou, J.P. Lin, G.L. Chen and P.K. Liaw, Adv. Eng. Mater. 10 (2008) pp.534–538.
- **15 F. Průša, M. Cabibbo, A. Šenková, V. Kučera, Z. Veselka, A. Školáková, D. Vojtěch, J. Cibulková and J. Čapek**, J. Alloys Compd. 835 (2020) p.155308.
- 16 J.W. Yeh, Ann. Chim. Sci. Mater. (Paris) 31 (2006) pp.633-648.
- 17 O.A. Waseem and H.J. Ryu, J. Alloys Compd. 828 (2020) p.154427.
- 18 N.N. Guo, L. Wang, L.S. Luo, X.Z. Li, R.R. Chen, Y.Q. Su, J.J. Guo and H.Z. Fu, Mater. Sci. Eng. A 651 (2016) pp.698–707.
- 19 N.N. Guo, L. Wang, L.S. Luo, X.Z. Li, R.R. Chen, Y.Q. Su, J.J. Guo and H.Z. Fu, Intermetallics 69 (2016) pp.13–20.
- 20 Y. Zhang, T.T. Zuo, Z. Tang, M.C. Gao, K.A. Dahmen, P.K. Liaw and Z.P. Lu, Prog. Mater. Sci. 61 (2014) pp.1–93.
- 21 J. Brechtl, S. Chen, C. Lee, Y. Shi, R. Feng, X. Xie, D. Hamblin, A.M. Coleman, B. Straka, H. Shortt, R. Jackson Spurling and P.K. Liaw, Metals. (Basel) 10 (2020) p.1101.
- 22 High-Entropy Alloys A New Era of Exploitation. Available at https://www.scientific.net/MSF.560.1.
- 23 O.N. Senkov, G.B. Wilks, D.B. Miracle, C.P. Chuang and P.K. Liaw, Intermetallics 18 (2010) pp.1758–1765.
- 24 O.N. Senkov, J.M. Scott, S.V. Senkova, D.B. Miracle and C.F. Woodward, J. Alloys Compd. 509 (2011) pp.6043–6048.
- **25 O.N. Senkov, J.M. Scott, S.V. Senkova, F. Meisenkothen, D.B. Miracle and C.F. Woodward**, J. Mater. Sci. 47 (2012) pp.4062–4074.
- **26 O.N. Senkov and C.F. Woodward**, Mater. Sci. Eng. A 529 (2011) pp.311–320.
- 27 O.N. Senkov, S.V. Senkova, D.M. Dimiduk, C. Woodward and D.B. Miracle, J. Mater. Sci. 47 (2012) pp.6522–6534.
- **28 P. Singh, A. Sharma, A.V. Smirnov, M.S. Diallo, P.K. Ray, G. Balasubramanian and D.D. Johnson**, npj Comput. Mater. 4 (2018) p.16.
- 29 A.V. Ayyagari, B. Gwalani, S. Muskeri, S. Mukherjee and R. Banerjee, npj Mater. Degrad. 2 (2018) p.33.
- **30 P. Lu, J.E. Saal, G.B. Olson, T. Li, O.J. Swanson, G.S. Frankel, A.Y. Gerard, K.F. Quiambao and J.R. Scully,** Scr. Mater. 153 (2018) pp.19–22.
- **31** K.F. Quiambao, S.J. McDonnell, D.K. Schreiber, A.Y. Gerard, K.M. Freedy, P. Lu, J.E. Saal, G.S. Frankel and J.R. Scully, Acta Mater. 164 (2019) pp.362–376.
- **32 J.S. Park, R. Sakidja and J.H. Perepezko**, Scr. Mater. 46 (2002) pp.765–770.
- 33 J.M. Ziman, Electrons and Phonons: The Theory of Transport Phenomena in Solids, OUP Oxford, Oxford, 2001.[Q3]
- **34 D.C. Wallace**, Am. J. Phys. 40 (1972) pp.1718–1719.
- 35 G.P. Srivastava, The Physics of Phonons, Routledge, Boca Raton, 2019.[Q4]
- 36 M.T. Dove and M.T. Dove, Introduction to Lattice Dynamics, Cambridge University Press, Cambridge, 1993.[Q5]
- **37 A. Togo, F. Oba and I. Tanaka**, Phys. Rev. B 78 (2008) p.134106.
- 38 J. Hafner, J. Comput. Chem. 29 (2008) pp.2044-2078.
- **39 N.D. Mermin**, Phys. Rev. 137 (1965) pp.A1441–A1443.
- 40 G. Kresse and D. Joubert, Phys. Rev. B Condens. Matter Mater. Phys.59 (1999) pp.1758-1775.
- **41 J.P. Perdew, K. Burke and M. Ernzerhof**, Phys. Rev. Lett. 77 (1996) pp.3865–3868.
- **42 M. Methfessel and A.T. Paxton**, Phys. Rev. B 40 (1989) pp.3616–3621.
- **43** H.J. Monkhorst and J.D. Pack, Phys. Rev. B 13 (1976) pp.5188–5192.
- 44 S.-H. Wei, L.G. Ferreira, J.E. Bernard and A. Zunger, Phys. Rev. B 42 (1990) pp.9622–9649.

- **45 G. Dirras, L. Lilensten, P. Djemia, M. Laurent-Brocq, D. Tingaud, J.-P. Couzinié, L. Perrière, T. Chauveau and I. Guillot,** Mater. Sci. Eng. A 654 (2016) pp.30–38.
- **46 Z.D. Han, N. Chen, S.F. Zhao, L.W. Fan, G.N. Yang, Y. Shao and K.F. Yao**, Intermetallics 84 (2017) pp.153–157.
- 47 R.P. Haggerty, P. Sarin, Z.D. Apostolov, P.E. Driemeyer and W.M. Kriven, J. Am. Ceram. Soc. 97 (2014) pp.2213–2222.
- **48 V.S. Babu, A.S. Pavlovic and M.S. Seehra**, Oxidation Characteristics and Thermal Expansion of Inconel Alloy 718 from 300 K to 1273 K, in Superalloys 718, 625, 706 and Various Derivatives (1997), 1997, pp. 689–693.

Processing math: 0%